Disposable gold coated pyramidal SERS sensor on the plastic platform

S. Z. Oo,[1,*] S. Siitonen,[2] V. Kontturi,[2] D. A. Eustace,[3] and M. D. B. Charlton[1]

[1]*School of Electronics & Computer Science, University of Southampton, Southampton, SO17 1BJ, UK*
[2]*Nanocomp Oy Ltd, Ensolantie 6, FI-80710, Lehmo, Finland*
[3]*Renishaw Diagnostics Ltd, Nova Technology Park, 5 Robroyston Oval, Glasgow, G33 1AP, UK*
[*]*S.Oo@soton.ac.uk*

Abstract: In this paper we investigate suitability of arrays of gold coated pyramids for surface-enhanced Raman scattering (SERS) sensing applications. Pyramidarrays composed of 1000nm pit size with 1250nm pitch lengthwerereplicated on a plastic substrate by roll-to-roll (R2R) ultraviolet (UV) embossing. The level of SERS enhancement, and qualitative performance provided by the new substrate is investigated by comparing Raman spectrum of benzenethiol (BTh) test molecules to the benchmark Klarite SERS substrate which comprises inverted pyramid arrays(1500nm pit size with 2000nm pitch length) fabricated on a silicon substrate. The new substrate is found to provide upto 11 times increase in signal in comparison to the inverted pyramid (IV-pyramid) arrays fabricated on an identical plastic substrate. Numerical simulation and experimental evidence suggest that strongly confined electromagnetic fields close to the base of the pyramids, are mainly responsible for the Raman enhancement factor, instead of the fields localized around the tip. Unusually strong plasmon fields are projected upto 200nm from the sidewalls at the base of the pyramid increasing the cross sectional sensing volume.

OCIS codes: (240.6695) Surface-enhanced Raman scattering; (130.6010) Sensors; (250.5403) Plasmonics.

References and links

1. B. Liu, G. Han, Z. Zhang, R. Liu, C. Jiang, S. Wang, and M.-Y. Han, "Shell thickness-dependent Raman enhancement for rapid identification and detection of pesticide residues at fruit peels," Anal. Chem. **84**(1), 255–261 (2012).
2. D. Volpati, P. H. B. Aoki, C. A. R. Dantas, F. V. Paulovich, M. C. F. de Oliveira, O. N. Oliveira, Jr., A. Riul, Jr., R. F. Aroca, and C. J. L. Constantino, "Toward the optimization of an e-tongue system using information visualization: a case study with perylene tetracarboxylic derivative films in the sensing units," Langmuir **28**(1), 1029–1040 (2012).
3. M. Özyürek, N. Güngör, S. Baki, K. Güçlü, and R. Apak, "Development of a silver nanoparticle-based method for the antioxidant capacity measurement of polyphenols," Anal. Chem. **84**(18), 8052–8059 (2012).
4. X. Wang, C. Wang, L. Cheng, S.-T. Lee, and Z. Liu, "Noble Metal coated single-walled carbon nanotubes for applications in surface enhanced raman scattering imaging and photothermal therapy," J. Am. Chem. Soc. **134**(17), 7414–7422 (2012).
5. K. Kaaki, K. Hervé-Aubert, M. Chiper, A. Shkilnyy, M. Soucé, R. Benoit, A. Paillard, P. Dubois, M.-L. Saboungi, and I. Chourpa, "Magnetic nanocarriers of doxorubicin coated with poly(ethylene glycol) and folic acid: relation between coating structure, surface properties, colloidal stability, and cancer cell targeting," Langmuir **28**(2), 1496–1505 (2012).
6. M. Delcea, N. Sternberg, A. M. Yashchenok, R. Georgieva, H. Bäumler, H. Möhwald, and A. G. Skirtach, "Nanoplasmonics for dual-molecule release through nanopores in the membrane of red blood cells," ACS Nano **6**(5), 4169–4180 (2012).
7. R. G. Freeman, K. C. Grabar, K. J. Allison, R. M. Bright, J. A. Davis, A. P. Guthrie, M. B. Hommer, M. A. Jackson, P. C. Smith, D. G. Walter, and M. J. Natan, "Self-assembled metal colloid monolayers: an approach to SERS substrates," Science **267**(5204), 1629–1632 (1995).
8. T. Qiu, W. Zhang, and P. K. Chu, "Recent progress in fabrication of anisotropic nanostructures for surface-enhanced Raman spectroscopy," Recent Pat. Nanotechnol. **3**(1), 10–20 (2009).

#252653 Received 6 Nov 2015; revised 2 Dec 2015; accepted 2 Dec 2015; published 8 Jan 2016

9. S. L. Smitha, K. G. Gopchandran, T. R. Ravindran, and V. S. Prasad, "Gold nanorods with finely tunable longitudinal surface plasmon resonance as SERS substrates," Nanotechnology **22**(26), 265705 (2011).
10. H. Chu, Y. Huang, and Y. Zhao, "Silver nanorod arrays as a surface-enhanced raman scattering substrate for foodborne pathogenic bacteria detection," Appl. Spectrosc. **62**(8), 922–931 (2008).
11. S. M. Prokes, O. J. Glembocki, R. W. Rendell, and M. G. Ancona, "Enhanced plasmon coupling in crossed dielectric/metal nanowire composite geometries and applications to surface-enhanced Raman spectroscopy," Appl. Phys. Lett. **90**(9), 093105 (2007).
12. T. Vo-Dinh, "Nanobiosensing Using Plasmonic Nanoprobes," IEEE J. Sel. Top. Quantum Electron. **14**(1), 198–205 (2008).
13. Y. Lu, G. L. Liu, J. Kim, Y. X. Mejia, and L. P. Lee, "Nanophotonic crescent moon structures with sharp edge for ultrasensitive biomolecular detection by local electromagnetic field enhancement effect," Nano Lett. **5**(1), 119–124 (2005).
14. J. Zhou, J. An, B. Tang, S. Xu, Y. Cao, B. Zhao, W. Xu, J. Chang, and J. R. Lombardi, "Growth of tetrahedral silver nanocrystals in aqueous solution and their SERS enhancement," Langmuir **24**(18), 10407–10413 (2008).
15. M. E. Abdelsalam, S. Mahajan, P. N. Bartlett, J. J. Baumberg, and A. E. Russell, "SERS at structured palladium and platinum surfaces," J. Am. Chem. Soc. **129**(23), 7399–7406 (2007).
16. L. Su, C. J. Rowlands, and S. R. Elliott, "Nanostructures fabricated in chalcogenide glass for use as surface-enhanced Raman scattering substrates," Opt. Lett. **34**(11), 1645–1647 (2009).
17. G. Das, N. Patra, A. Gopalakrishnan, R. P. Zaccaria, A. Toma, S. Thorat, E. Di Fabrizio, A. Diaspro, and M. Salerno, "Fabrication of large-area ordered and reproducible nanostructures for SERS biosensor application," Analyst (Lond.) **137**(8), 1785–1792 (2012).
18. G. Das, E. Battista, G. Manzo, F. Causa, P. A. Netti, and E. Di Fabrizio, "Large-scale plasmonic nanocones array for spectroscopy detection," ACS Appl. Mater. Interfaces **7**(42), 23597–23604 (2015).
19. F. De Angelis, M. Patrini, G. Das, I. Maksymov, M. Galli, L. Businaro, L. C. Andreani, and E. Di Fabrizio, "A hybrid plasmonic-photonic nanodevice for label-free detection of a few molecules," Nano Lett. **8**(8), 2321–2327 (2008).
20. E. J. Blackie, E. C. Le Ru, and P. G. Etchegoin, "Single-molecule surface-enhanced Raman spectroscopy of nonresonant molecules," J. Am. Chem. Soc. **131**(40), 14466–14472 (2009).
21. E. C. Le Ru, P. G. Etchegoin, and M. Meyer, "Enhancement factor distribution around a single surface-enhanced Raman scattering hot spot and its relation to single molecule detection," J. Chem. Phys. **125**(20), 204701 (2006).
22. K. A. Willets and R. P. Van Duyne, "Localized surface plasmon resonance spectroscopy and sensing," Annu. Rev. Phys. Chem. **58**(1), 267–297 (2007).
23. N.-J. Kim, M. Lin, Z. Hu, and H. Li, "Evaporation-controlled chemical enhancement of SERS using a soft polymer substrate," Chem. Commun. (Camb.) (**41**), 6246–6248 (2009).
24. X. Yu, H. Cai, W. Zhang, X. Li, N. Pan, Y. Luo, X. Wang, and J. G. Hou, "Tuning chemical enhancement of SERS by controlling the chemical reduction of graphene oxide nanosheets," ACS Nano **5**(2), 952–958 (2011).
25. R. A. Tripp, R. A. Dluhy, and Y. Zhao, "Novel nanostructures for SERS biosensing," Nano Today **3**(3-4), 31–37 (2008).
26. A. J. Haes, C. L. Haynes, A. D. McFarland, G. C. Schatz, R. P. Van Duyne, and S. Zou, "Plasmonic Materials for Surface-Enhanced Sensing and Spectroscopy," MRS Bull. **30**(05), 368–375 (2005).
27. C.-C. Ho, K. Zhao, and T.-Y. Lee, "Quasi-3D gold nanoring cavity arrays with high-density hot-spots for SERS applications via nanosphere lithography," Nanoscale **6**(15), 8606–8611 (2014).
28. Y. Weisheng, W. Zhihong, Y. Yang, C. Longqing, S. Ahad, W. Kimchong, and W. Xianbin, "Electron-beam lithography of gold nanostructures for surface-enhanced Raman scattering," J. Micromech. Microeng. **22**(12), 125007 (2012).
29. Y. Choi, S. Hong, and L. P. Lee, "Shadow overlap ion-beam lithography for nanoarchitectures," Nano Lett. **9**(11), 3726–3731 (2009).
30. S. Y. Chou, P. R. Krauss, and P. J. Renstrom, "Imprint of sub-25 nm vias and trenches in polymers," Appl. Phys. Lett. **67**(21), 3114–3116 (1995).
31. M. Cottat, N. Lidgi-Guigui, I. Tijunelyte, G. Barbillon, F. Hamouda, P. Gogol, A. Aassime, J.-M. Lourtioz, B. Bartenlian, and M. L. de la Chapelle, "Soft UV nanoimprint lithography-designed highly sensitive substrates for SERS detection," Nanoscale Res. Lett. **9**(1), 2361 (2014).
32. S. Kim, Y. Xuan, V. P. Drachev, L. T. Varghese, L. Fan, M. Qi, and K. J. Webb, "Nanoimprinted plasmonic nanocavity arrays," Opt. Express **21**(13), 15081–15089 (2013).
33. S.-W. Lee, K.-S. Lee, J. Ahn, J.-J. Lee, M.-G. Kim, and Y.-B. Shin, "Highly sensitive biosensing using arrays of plasmonic Au nanodisks realized by nanoimprint lithography," ACS Nano **5**(2), 897–904 (2011).
34. C. J. Choi, Z. Xu, H. Y. Wu, G. L. Liu, and B. T. Cunningham, "Surface-enhanced Raman nanodomes," Nanotechnology **21**(41), 415301 (2010).
35. M. Hu, F. S. Ou, W. Wu, I. Naumov, X. Li, A. M. Bratkovsky, R. S. Williams, and Z. Li, "Gold nanofingers for molecule trapping and detection," J. Am. Chem. Soc. **132**(37), 12820–12822 (2010).
36. G. Kostovski, D. J. White, A. Mitchell, M. W. Austin, and P. R. Stoddart, "Nanoimprinted optical fibres: Biotemplated nanostructures for SERS sensing," Biosens. Bioelectron. **24**(5), 1531–1535 (2009).
37. R. Alvarez-Puebla, B. Cui, J.-P. Bravo-Vasquez, T. Veres, and H. Fenniri, "Nanoimprinted SERS-active substrates with tunable surface plasmon resonances," J. Phys. Chem. C **111**(18), 6720–6723 (2007).

#252653 Received 6 Nov 2015; revised 2 Dec 2015; accepted 2 Dec 2015; published 8 Jan 2016

38. Z. Xu, H.-Y. Wu, S. U. Ali, J. Jiang, B. T. Cunningham, and G. L. Liu, "Nanoreplicated positive and inverted submicrometer polymer pyramid array for surface-enhanced Raman spectroscopy," NANOP **5**, 053526–053526–053511 (2011).
39. S. Z. Oo, R. Y. Chen, S. Siitonen, V. Kontturi, D. A. Eustace, J. Tuominen, S. Aikio, and M. D. B. Charlton, "Disposable plasmonic plastic SERS sensor," Opt. Express **21**(15), 18484–18491 (2013).
40. P. Karioja, J. Hiltunen, S. Aikio, T. Alajoki, J. Tuominen, M. Hiltunen, S. Siitonen, V. Kontturi, K. Böhlen, R. Hauser, M. Charlton, A. Boersma, P. Lieberzeit, T. Felder, D. Eustace, and E. Haskal, "Toward large-area roll-to-roll printed nanophotonic sensors," Proc. SPIE **9141**, 91410D (2014).
41. S. Z. Oo, M. D. B. Charlton, D. Eustace, R. Y. Chen, S. J. Pearce, and M. E. Pollard, "Optimization of SERS enhancement from nanostructured metallic substrate based on arrays of inverted rectangular pyramids and investigation of effect of lattice non-symmetry," Proc. SPIE **8234**, 823406 (2012).
42. S. Z. Oo, M. D. B. Charlton, M. E. Pollard, S. J. Pearce, and R. Y. Chen, "3D analysis of surface plasmon dispersion for SERS sensor based on inverted pyramid nanostructures," Proc. SPIE **8269**, 82691Y (2012).
43. M. R. Gartia, Z. Xu, E. Behymer, H. Nguyen, J. A. Britten, C. Larson, R. Miles, M. Bora, A. S. Chang, T. C. Bond, and G. L. Liu, "Rigorous surface enhanced Raman spectral characterization of large-area high-uniformity silver-coated tapered silica nanopillar arrays," Nanotechnology **21**(39), 395701 (2010).
44. S. Mathias, E. C. Filho, and R. G. Cecchini, "The dipole moments of cyclohexanethiol, α-toluenethiol and benzenethiol," J. Phys. Chem. **65**(3), 425–427 (1961).
45. J. Y. Gui, D. A. Stern, D. G. Frank, F. Lu, D. C. Zapien, and A. T. Hubbard, "Adsorption and surface structural chemistry of thiophenol, benzyl mercaptan, and alkyl mercaptans. Comparative studies at silver(111) and platinum(111) electrodes by means of Auger spectroscopy, electron energy loss spectroscopy, low energy electron diffraction and electrochemistry," Langmuir **7**(5), 955–963 (1991).
46. N. M. B. Perney, J. J. Baumberg, M. E. Zoorob, M. D. B. Charlton, S. Mahnkopf, and C. M. Netti, "Tuning localized plasmons in nanostructured substrates for surface-enhanced Raman scattering," Opt. Express **14**(2), 847–857 (2006).
47. M. C. Netti, M. E. Zoorob, M. D. Charlton, P. Ayliffe, S. Mahnkopf, P. Stopford, K. Todd, J. R. Lincoln, N. M. B. Perney, and J. J. Baumberg, "Probing molecules by surface-enhanced Raman spectroscopy," Proc. SPIE **6093**, 60930F (2006).

1. Introduction

In recent years there has been an increasing interest in analysis and identification of complex molecules for the medical diagnostics, pharmaceutical research and homeland security applications [1–6]. If these molecules are present in high concentration, a technique known as Raman spectroscopy can be utilized. Unfortunately, only one in every 10^{12} photon incidence on molecule undergoes Raman scattering resulting in weak Raman absorption. An efficient technique to overcome this limitation is to utilize surface-enhanced Raman scattering (SERS) whereby molecules are placed on the surface of nanostructured metallic substrate which performs the function of transducting photon into and out of the molecules. SERS extends the scope of Raman scattering to detect molecules at low concentrations to few/single molecule level. Various SERS substrates with different materials [7–22] have been researched and claimed to have electromagnetic enhancement in the range 10^{8}- 10^{13} while the chemical enhancement [23,24] has also been reported in several cases for the low order of enhancement ($\sim 10^{2}$-10^{4}). Most of these SERS substrates are commonly based on the silicon platform using the conventional fabrication techniques such as optical (ultraviolet) lithography, electron beam lithography and focused ion beam lithography which are not cost effective and have low throughput for mass production [25–29]. Thus an alternative lithography process has been demanded to fulfill low cost mass manufacturing for industrial application. Nanoimprint lithography becomes an alternative solution due to its simple, cost-effective and high throughput for replicating micro/nano-structures since it was introduced in 1995 by S.Y. Chou et.al [30]. Therefore, recently SERS researchers have taken interest in replicating the micro- and nano-structures using nano-imprinting [31–38]. In this paper we present a new high performance plastic SERS sensor which was replicated from an optimized and enhanced version of the Klarite SERS substrate. Conventional Klarite is based on inverted pyramids with 2000nm pitch length and 1500nm pit size, has simple square cross section and is fabricated on a silicon platform. Our modified (and optimized) version of Klarite consists of inverted pyramidal arrays with 1250nm pitch length and 1000nm pit size, but with rectangular cross sections of various aspect ratio. A plastic replication of Klarite has been researched by

#252653 Received 6 Nov 2015; revised 2 Dec 2015; accepted 2 Dec 2015; published 8 Jan 2016

Xu et.al [38] and the enhancement factors of the replicated polymer substrates for inverted (IV) pyramid and pyramid has been shown as $1.6x10^6$ and $7.2x10^4$ respectively for a Benzenthiol (BTh) test molecule. From the enhanced silicon version of Klarite, plastic substrates have been replicated into two different forms called inverted (IV) pyramid andpyramid by nanoimprinting. In this paper wediscuss only on the plastic pyramid since the discussion on the IV plastic pyramid has been published previously [39]. Thepyramid polymer SERS substrate demonstrates excellent qualitative enhancement of Raman amplification for the BTh molecule of $7.20x10^7$and has the great potential in view of simple replication and mass manufacturing.

2. Sample preparation

A pyramidal array was replicated on a plastic substrate, Poly methyl methacrylate (PMMA) by Roll to Roll (R2R) UV embossing [40] which has great potential for low-cost high volume production. Firstly a silicon master stamp of an array of atomically smooth inverted pyramidal rectangular pits is fabricated, by electron-beam lithography and anisotropic wet chemical etching of <111> planes through rectangular openings in a silicon dioxide mask on a <100> oriented silicon wafer. The fabricated mold used in this work contains an array of inverted pyramids etched into a 8mm x 8mm area with inverted pyramids of 1000nm x 1250nm rectangle, 706nm deep with a pitch of 1250nm, as shown in Fig. 1(a).Then a plastic replica made by the imprinting process. We used NanoCompOyLtd's propriatory acrylate based UV curable lacquer polymers for nano-imprinting. Since we use UV curing process rather than hot embossing, there is no need for high pressure imprinting, and there are no thermal or melting issues. The geometry consisted of arrays of inverted rectangular shaped pyramids with 1000nm pit size, 1250nm pitch length, 1:1.2 width to length aspect ratio, and 328.5nm (measured) gold thickness. Gold deposition was carried out using a bespoke Leybold electron-beam evaporator system. The gold coated sample was examined under the scanning electron microscope, SEM(JSM 7500F FEGSEM, JEOL Ltd.) verifying that the gold coating had uniform (10nm scale) roughness both on the sidewall and flat surface between neighboring pits as shown in Fig. 1(b).

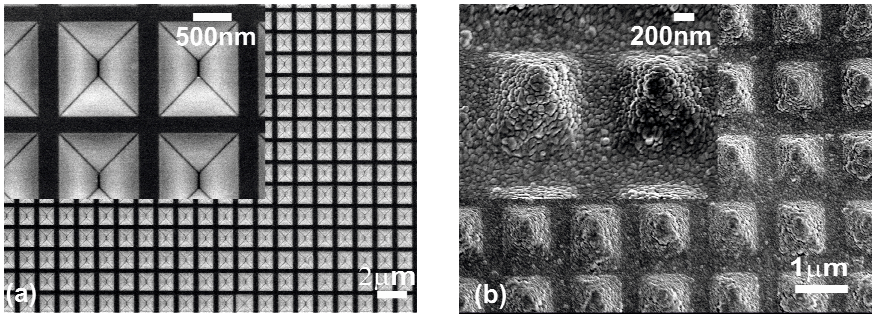

Fig. 1. (a) SEM image for silicon master (b) SEM image for plastic replicated pyramidal arrays. Insets are for the high magnification view for the substrate.

To investigate the enhanced Raman effect from pyramid arrays, a Benzenethiol, BTh (C_6H_5SH) test molecule was coated on the sample by immersing the substrate overnight in 5mM BTh solution in ethanol, allowing the SH group to bind with gold surface and form a closely packed monolayer. Excess BTh molecules were then washed off by thoroughly rinsing in ethanol solution. The substrate was then examined again by SEM showing that a relatively thick layer of molecules has taken up the space between the bottom of the pyramids and the flat surface between the pyramids instead of forming a thin conformal mono-layer on the pyramid sidewall. This is most likely due to combination of gravity and capillary action causing self- concentration of BTh molecules during the drying process.

#252653 Received 6 Nov 2015; revised 2 Dec 2015; accepted 2 Dec 2015; published 8 Jan 2016

3. Results and discussion

3.1 Raman characterization

Raman measurements were performed using a RenishawInvia Raman system at 785nm excitation wavelength with 44mW power, 3sec exposure time, 2 times accumulation, 5 times objective lens with NA = 0.12. The advantage of using lower maginification is that the stray light from surrounding can be collected. However, the points of using lower magnification objective in this work are as follows: (1). With regards to illuminated area, there is a tradeoff between measured Raman intensity and measurement signal reproducibility depending on area of illumination. Using the smaller laser spot size with higher magnification will illuminate a small area within a single pyramid.For the purpose of obtaining reliable repeatable measurement it is better to illuminate at least one full pyramid, but better still several pyramids in order to get an 'averaged' measurement reading. This approach avoids small varation in Raman signal due to small differences in molecular or gold coating between adjacent pits. (2). Using the lower magnification can gives a lower optical power density at the substrate surface which is suitable for organic and biological molecules without damaging them. (3) Low power density enables us to demonstrate suitability of the plastic pyramid SERS sensor for low power measurement.

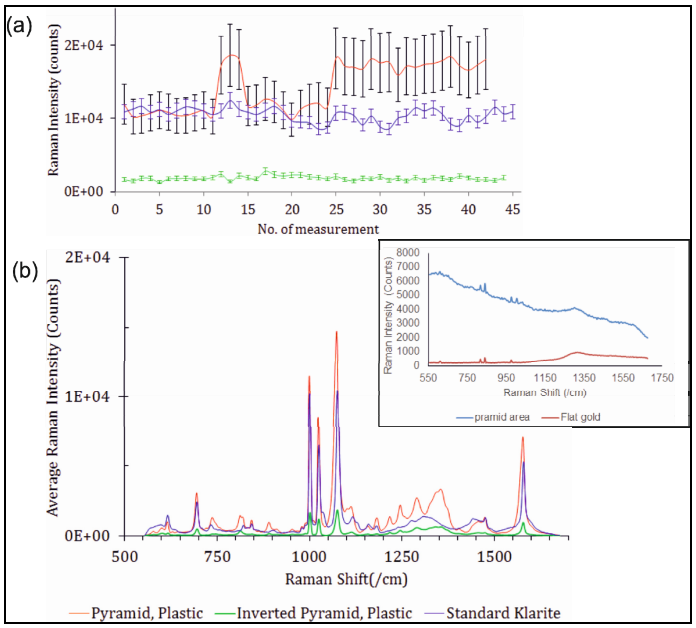

Fig. 2. (a) Point to point reproducibility calculated at the 1075cm^{-1} Raman vibrational frequency of BTh molecules for the different substrates, error bars represent the relative standard deviation from its average Raman intensity. (b) Average Raman spectra of BTh molecules after 45 measurements on each chip for the different substrates. Inset shows Raman spetra from plastic substrate before molecule coating which are used as reference signal.

Measurements were taken at 45 random points across an 8mmx8mm chip area. Figure 2(a) shows each individual measurement of the 1075cm^{-1} vibrational frequency of the BTh molecule for each substrate, and allows us to visually compare point to point measurement repeatability, which is important for a commercially viable sensor. The error bars show relative standard deviation from the average Raman intensity for each measurement. Figure 2(b) shows Raman spectra averaged over all measurement points for several different types of pyramidal SERS substrate. Inset shows Raman spetra from plastic substrate before molecule coating which are used as reference signal. Each was fabricated under identical conditions

#252653 Received 6 Nov 2015; revised 2 Dec 2015; accepted 2 Dec 2015; published 8 Jan 2016

and materials for the purpose of relative performance comparison. These include: pyramid and IV pyramid in the plastic platform, standard Klarite (square shaped inverted pyramids arranged on a square grid in silicon substrate). Full details of these test substrates are given in previous publication [39, 41 ,42] and so are not repeated here.

For clarity, average Raman signal intensity for the main vibrational frequencies of BTh molecules are tabulated in Table 1 for comparison. We see from this data that pyramid design provides 8 to 12 fold enhancement of Raman amplification (dependent on Raman peak) compared to IV-pyramid design on the same plastic substrate. The enhancement factor and reproducibility is tabulated in Table 2 using C-C stretch mode of BTh. The enhancement factor is calculated using the equation introduced by Dr. R. L. Aggarwal and his colleagues [43, 44]:

$$EF = \frac{I_{SERS}}{I_{RS}} \times \frac{N \times L}{N_A \times m} \times \frac{1}{n^2} \tag{1}$$

which considered the increased surface area of the nanostructured surface under the laser illuminated area. In Eq. (1), I_{SERS} is the Raman intensity from the SERS substrate and I_{RS} are for the Raman intensity from the bulk molecules, N is the molecular density of test molecule and N_A is the areal density of test molecules on flat surface, L is the Raman scattering length, m is the areal multiplier and n is the refractive index of test molecule. Substituting the values of n = 1.56 [40], N = $5.9 \times 10^{21} cm^{-3}$ [43], $N_A = 3.3 \times 10^{14} cm^{-2}$ [45]on flat surface, L = 0.9mm at which the intensity decays exponentially to 50% of the maximum value for x5 objective lens with 0.12 numerical aperture and m = 1.29 for the illuminated area $10202 \mu m^2$ covering approximately the number of pyramid, 5441 where 'm' is calculated using the equation:

$$m = \frac{Area + [B(2C + 2D)] - (B \times E)}{Area} \tag{2}$$

where "Area" is for the illuminated area by the excitation laser, B is for the number of pyramids covered by the illuminated area, C and D are for the area of triangle and trapezium respectively and E is for the area of based rectangle of the pyramid.

Table 1. Comparison of Average Raman Intensity for the Characteristic Vibrational Modes of BTh Molecules on Different Substrates

Characteristic Raman Vibrational frequencies of BTh molecules (/cm)	*Average Raman Intensity (Counts)*		
	Pyramid, Plastic	*IV-Pyramid, Plastic*	*Standard Klarite*
Ring deformation (615-630)	1183.82	173.73	1312.38
Trigonal ring breathing (990-1010)	18511.34	1483.73	10212.66
In-plane CH deformation (1015-1030)	8243.21	901.42	6494.39
CC stretches, 1075	17484.44	1554.25	10483.99
Ring stretches (1550-1630)	7046.96	700.65	5301.01

We find that pyramid plastic device has a point to point variation of 22%, which is more than twice that of standard Klarite. We believe that this may be due to lack of uniformity in test molecule coating over the substrate surface as shown in the SEM image (Figs. 1(b)). Overall, performance in terms of Raman intensity and enhancement factor provided by the new pyramidplastic device is competitive to the benchmark silicon Klarite (with the same metallization condition), with a factor of 1.66 improvements for the C-C stretch mode of the test molecule where the areal multiplier, m is 1.231 for the standard Klarite.

#252653 Received 6 Nov 2015; revised 2 Dec 2015; accepted 2 Dec 2015; published 8 Jan 2016

Table 2. Qualitative and Quantitative Performance of the Different SERS Substrates at C-C Stretch Mode of BTh

Substrates	*Enhancement Factor (EF)*	*Reproducibility (%)*
Pyramid, plastic *(EN)*	7.2×10^7	22.88
IV-pyramid, plastic *(EN)*	6.38×10^6	16.02
Standard Klarite	4.54×10^7	8.88

"EN" refers to the enhanced design of Klarite. Note that the areal multiplier for enhanced inverted pyramid of plastic is used the same multiplier value of the pyramid because it does not need to count the volume of the cavity mode of inverted pyramid due to the monolayer of BTh molecules assembling only on the sidewalls of the inverted pyramid. If the coated unknown molecule is a kind that can fill up the volume within the cavity of inverted pyramid, the areal multiplier 'm' for the inverted pyramid will be used as 0.563.

3.2 Simulation

To investigate which artefact of the substrate geometry is responsible for the enhancement of the Raman amplification, the pyramidal array was modelled using 'RSoft Photonic Suite', DiffractMOD simulator in which Rigorous Coupled Wave Algorithm (RCWA) and the periodic boundary condition are applied to collect the zero order diffraction and spatial e-field as a figure of merit. It is generally believed that SERS signals are related to the localized surface plasmons which are formed by electron oscillation at the interface between the metal and the dielectric. In combination with this, nm scale granularity of the gold surface plays a huge role in channeling optical energy efficiently into the test molecules. In the simulation field intensity monitors covering the surface area of 2.5x2.958 μm^2, are placed at several vertical positions (heights) above the base of the pyramids. The monitor records the e-field as function of spatial position at the excitation wavelength of 785nm according to:

$$U_E\left(r'\right) = \frac{1}{2}\mathrm{Re}\left[\varepsilon\left(r'\right)\right]\left|E\left(r'\right)\right|^2 \tag{3}$$

Where E is the electric field, ε is the spatially dependent index and r′ is the spatial coordinate. The monitor grid size is 1nm resolution to cover the detail shape of the pyramid.

Eight e-field monitors were placed 100nm apart each from the base of the pyramid till reaching the tip of the pyramid. Results are shown in Fig. 3. Example field plots taken at 0nm, 300nm and 700nm height above the pyramid base are shown in Figs. 3(c)-3(e). We see from Figs. 3(c)-3(e) that the e-field is predominantly localized to the base of the sidewalls of the pyramids and there is very little localization of e-field in the large space between the pyramids. Figure 3(b) plots the total e-field energy integrated across the area of each monitor, as a function of height from the base of the pyramid. It is clear that the maximum electric field is experienced at 300nm height from the base of the pyramid, and not the tip of the pyramid. These results suggest that for the pyramid geometry, the bulk of the Raman enhancement occurs in the region of space close to the base of the pyramid where the e-field is localized and is able to interact strongly with the concentrated molecules. This is surprising because the tip of the pyramid is widely believed to provide the largest field strength and so would intuitively be expected to provide the main SERS enhancement. Furthermore, we note that there is very little field localized to the large space between the pyramids. Consequently, there cannot be much contribution to Raman enhancement arising from interactions with dispersive surface plasmons [41, 42] which normally become localized to the space between the IV-pyramids. This is in contrast to standard Klarite where the low group velocity propagating plasmons play a role [46, 47]. Also, the difference in the field distribution between the pyramid and inverted pyramid on the identical plastic platform was studied as a spatial electric field across the center of the pyramid as shown in Fig. 3(f) and 3(g),

#252653 Received 6 Nov 2015; revised 2 Dec 2015; accepted 2 Dec 2015; published 8 Jan 2016

respectively. Both field distributions occurred on the sidewall which enhances the Raman amplification of the molecules deposited on the sidewall. Again this confirms that the e-field at the tip of the pyramid was lower compared to that at the base.

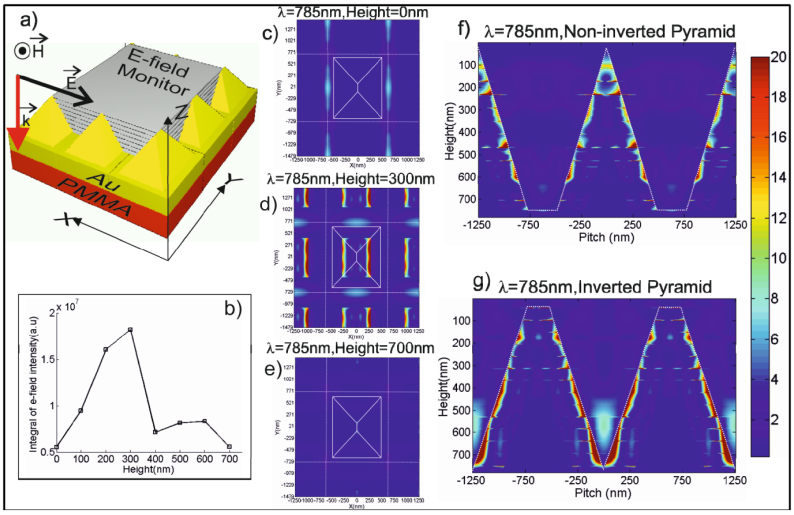

Fig. 3. The variation of the e-field distribution along the height of the pyramid array, (a) illustration for the simulated 3D pyramidal array, the gray rectangular box representing the covered area to monitor the field intensity varied with the height. (b) a line graph shows the total integral of the e-field intensity over each monitored area as a function of height above the base of the pyramid. (c), (d) and (e) are the e-field distribution at the height of 0nm, 300nm and 700nm above the base of the pyramid, respectively. (g) is the e-field distribution of the cross-sectional view for the pyramid.

4. Conclusion

We have demonstrated that a plastic SERS sensorutilizing arrays of gold coated pyramids canprovide a viable SERS sensing substrate, and shows upto 11 times higher SERS enhancement compared to conventional inverted pyramid geometry on a ‘like for like’ plastic platform, using the same test molecules and measurement parameters. Previously [39] we have shown that a plastic platform sensor using inverted pyramids provides poor performance compared to its silicon counter-part ‘Klarite’ (comparative experiments were repeated in this study), although this can be compensated by optimizing the geometry and metallization process. Despite this, the qualitative performance of the new plastic substrate is comparable to the benchmark silicon based Klarite SERS substrate. The new plastic sensor was fabricated by nano-imprint lithography onto a flexible plastic substrate, which is highly suitable for low cost high volume manufacturing. Simulation results showed that the e-field is strongly confined to the base of the pyramid walls. Fortuitously, self-concentration effects during analyte drying process are likely to increase cross section of interaction with test molecules for this geometry. Presented SEM imagesand simulations showthat the moleculesbecome dissipated atthe height as maximum e-field strength.We believe that this is the primary reason for the strong enhancement of Raman signature of the deposited molecule. In the simulation we also observe that the e-field at the tip of the pyramid is not as strong as the base of the pyramid.

Acknowledgments

We acknowledge the financial support from the FP7 ‘PHOTOSENS’ consortium project (FP7-NMP-2010-LARGE-4-263382).

#252653 Received 6 Nov 2015; revised 2 Dec 2015; accepted 2 Dec 2015; published 8 Jan 2016